Giant tunable optical dispersion using chromo-modal excitation of a multimode waveguide

Eric D. Diebold,[1,2,*] Nick K. Hon,[1,2] Zhongwei Tan,[1,7] Jason Chou,[1,5] Todd Sienicki,[1,6] Chao Wang,[1,2] and Bahram Jalali[1,2,3,4]

[1]*Electrical Engineering Department, University of California, Los Angeles, CA 90095, USA*
[2]*California NanoSystems Institute, Los Angeles, CA 90095, USA*
[3]*Department of Bioengineering, University of California, Los Angeles, CA 90095, USA*
[4]*Department of Surgery, David Geffen Schools of Medicine, University of California, Los Angeles, CA 90095, USA*
[5]*Current address: Lawrence Livermore National Laboratory, Livermore, CA, USA*
[6]*Current address: Lasson Technologies Inc., San Diego, CA, USA*
[7]*Permanent address: Institute of Lightwave Technology, Beijing Jiaotong University, Beijing 100044, China*
**ediebold@ucla.edu*

Abstract: The ability to control chromatic dispersion is paramount in applications where the optical pulsewidth is critical, such as chirped pulse amplification and fiber optic communications. Typically, devices used to generate large amounts (>100 ps/nm) of chromatic dispersion are based on diffraction gratings, chirped fiber Bragg gratings, or dispersion compensating fiber. Unfortunately, these dispersive elements suffer from one or more of the following restrictions: (i) limited operational bandwidth, (ii) limited total dispersion, (iii) low peak power handling, or (iv) large spatial footprint. Here, we introduce a new type of tunable dispersive device, which overcomes these limitations by leveraging the large modal dispersion of a multimode waveguide in combination with the angular dispersion of diffraction gratings to create chromatic dispersion. We characterize the device's dispersion, and demonstrate its ability to stretch a sub-picosecond optical pulse to nearly 2 nanoseconds in 20 meters of multimode optical fiber. Using this device, we also demonstrate single-shot, time-wavelength atomic absorption spectroscopy at a repetition rate of 90.8 MHz.

OCIS codes: (260.2030) Dispersion; (130.2035) Dispersion compensation devices; (320.7150) Ultrafast spectroscopy; (320.7160) Ultrafast technology; (300.6530) Spectroscopy, ultrafast; (230.7370) Waveguides.

References and links:

1. D. Strickland and G. Mourou, "Compression of amplified chirped optical pulses," Opt. Commun. **56**(3), 219–221 (1985).
2. G. A. Mourou, T. Tajima, and S. V. Bulanov, "Optics in the relativistic regime," Rev. Mod. Phys. **78**(2), 309–371 (2006).
3. M. D. Perry and G. Mourou, "Terawatt to petawatt subpicosecond lasers," Science **264**(5161), 917–924 (1994).
4. A. H. Zewail, "Femtochemistry: atomic-scale dynamics of the chemical bond," J. Phys. Chem. A **104**(24), 5660–5694 (2000).
5. R. R. Gattass and E. Mazur, "Femtosecond laser micromachining in transparent materials," Nat. Photonics **2**(4), 219–225 (2008).
6. T. H. Her, R. J. Finlay, C. Wu, S. Deliwala, and E. Mazur, "Microstructuring of silicon with femtosecond laser pulses," Appl. Phys. Lett. **73**(12), 1673–1675 (1998).
7. M. D. Shirk and P. A. Molian, "A review of ultrashort pulsed laser ablation of materials," J. Laser Appl. **10**(1), 18–28 (1998).
8. D. E. Spence, P. N. Kean, and W. Sibbett, "60-fsec pulse generation from a self-mode-locked Ti:sapphire laser," Opt. Lett. **16**(1), 42–44 (1991).
9. D. R. Solli, J. Chou, and B. Jalali, "Amplified wavelength-time transformation for real-time spectroscopy," Nat. Photonics **2**(1), 48–51 (2008).
10. D. R. Solli, C. Ropers, P. Koonath, and B. Jalali, "Optical rogue waves," Nature **450**(7172), 1054–1057 (2007).

#155170 - $15.00 USD Received 26 Sep 2011; revised 21 Oct 2011; accepted 23 Oct 2011; published 8 Nov 2011

11. F. Coppinger, A. S. Bhushan, and B. Jalali, "Photonic time stretch and its application to analog-to-digital conversion," IEEE Trans. Microw. Theory Tech. **47**(7), 1309–1314 (1999).
12. Y. Han and B. Jalali, "Photonic time-stretched analog-to-digital converter: fundamental concepts and practical considerations," J. Lightwave Technol. **21**(12), 3085–3103 (2003).
13. W. J. Caputi, "Stretch: A time-transformation technique," IEEE Trans. Aerosp. Electron. Syst. **AES-7**(2), 269–278 (1971).
14. B. H. Kolner, "Space-time duality and the theory of temporal imaging," IEEE J. Quantum Electron. **30**(8), 1951–1963 (1994).
15. C. V. Bennett and B. H. Kolner, "Upconversion time microscope demonstrating 103 x magnification of femtosecond waveforms," Opt. Lett. **24**(11), 783–785 (1999).
16. M. A. Foster, R. Salem, D. F. Geraghty, A. C. Turner-Foster, M. Lipson, and A. L. Gaeta, "Silicon-chip-based ultrafast optical oscilloscope," Nature **456**(7218), 81–84 (2008).
17. K. Goda, K. K. Tsia, and B. Jalali, "Serial time-encoded amplified imaging for real-time observation of fast dynamic phenomena," Nature **458**(7242), 1145–1149 (2009).
18. A. Mahjoubfar, K. Goda, A. Ayazi, A. Fard, S. H. Kim, and B. Jalali, "High-speed nanometer-resolved imaging vibrometer and velocimeter," Appl. Phys. Lett. **98**(10), 101107 (2011).
19. D. Derickson, *Fiber Optic Test and Measurement* (Prentice Hall, Upper Saddle River, NJ, 1998).
20. W. A. Gambling, D. N. Payne, and H. Matsumura, "Mode conversion coefficients in optical fibers," Appl. Opt. **14**(7), 1538–1542 (1975).
21. D. Gloge, "Optical Power Flow in Multimode Fibers," Bell Syst. Tech. J. **51**, 1767 (1972).
22. M. D. Perry, R. D. Boyd, J. A. Britten, D. Decker, B. W. Shore, C. Shannon, and E. Shults, "High-efficiency multilayer dielectric diffraction gratings," Opt. Lett. **20**(8), 940–942 (1995).
23. J. Chou, D. R. Solli, and B. Jalali, "Real-time spectroscopy with subgigahertz resolution using amplified dispersive Fourier transformation," Appl. Phys. Lett. **92**(11), 111102 (2008).
24. P. V. Kelkar, F. Coppinger, A. S. Bhushan, and B. Jalali, "Time-domain optical sensing," Electron. Lett. **35**(19), 1661–1662 (1999).
25. D. R. Solli, S. Gupta, and B. Jalali, "Optical phase recovery in the dispersive Fourier transform," Appl. Phys. Lett. **95**(23), 231108 (2009).
26. K. Goda, D. R. Solli, K. K. Tsia, and B. Jalali, "Theory of amplified dispersive Fourier transformation," Phys. Rev. A **80**(4), 043821 (2009).
27. W. B. Jones, *Introduction to Optical Fiber Communication Systems* (Oxford University Press, New York, 1998).
28. E. B. Treacy, "Optical pulse compression with diffraction gratings," IEEE J. Quantum Electron. **5**(9), 454–458 (1969).
29. O. E. Martinez, "3000 times grating compressor with positive group-velocity dispersion - application to fiber compensation in 1.3-1.6 μm region," IEEE J. Quantum Electron. **23**(1), 59–64 (1987).
30. M. Y. Shverdin, F. Albert, S. G. Anderson, S. M. Betts, D. J. Gibson, M. J. Messerly, F. V. Hartemann, C. W. Siders, and C. P. J. Barty, "Chirped-pulse amplification with narrowband pulses," Opt. Lett. **35**(14), 2478–2480 (2010).
31. B. Temelkuran, S. D. Hart, G. Benoit, J. D. Joannopoulos, and Y. Fink, "Wavelength-scalable hollow optical fibres with large photonic bandgaps for CO_2 laser transmission," Nature **420**(6916), 650–653 (2002).
32. J. P. Koplow, D. A. V. Kliner, and L. Goldberg, "Single-mode operation of a coiled multimode fiber amplifier," Opt. Lett. **25**(7), 442–444 (2000).
33. A. Galvanauskas, "Mode-scalable fiber-based chirped pulse amplification systems," IEEE J. Sel. Top. Quantum Electron. **7**(4), 504–517 (2001).
34. L. Chi-Hung, C. Guoqing, L. Natasha, G. Almantas, G. Doug, J. Nick and T. Kanishka, "Effectively single-mode chirally-coupled core fiber," in *Advanced Solid-State Photonics*, OSA Technical Digest Series (CD) (Optical Society of America, 2007), paper ME2.
35. H. Bulow, F. Buchali, and A. Klekamp, "Electronic dispersion compensation," J. Lightwave Technol. **26**(1), 158–167 (2008).
36. E. Ip and J. M. Kahn, "Digital equalization of chromatic dispersion and polarization mode dispersion," J. Lightwave Technol. **25**(8), 2033–2043 (2007).
37. S. J. Savory, G. Gavioli, R. I. Killey, and P. Bayvel, "Electronic compensation of chromatic dispersion using a digital coherent receiver," Opt. Express **15**(5), 2120–2126 (2007).

1. Introduction

Dispersive optical elements play critical roles in the operation of many high-bandwidth optical systems. The ability to stretch and compress optical pulses using chromatic, or group velocity, dispersion (GVD) forms the basis for chirped pulse amplification (CPA) – an indispensable technique for amplifying ultra-short optical pulses [1]. Today, the use of high-energy ultra-short laser pulses is pervasive in applications ranging from basic scientific research [2–4] to industrial material processing [5–7]. An even more ubiquitous use of GVD is dispersion compensation in high bit-rate optical communication networks, which form the

#155170 - $15.00 USD Received 26 Sep 2011; revised 21 Oct 2011; accepted 23 Oct 2011; published 8 Nov 2011

backbone of the Internet. In this case, dispersion management is critical for controlling data impairment caused by optical dispersion and nonlinearities. Other important applications of GVD include intracavity dispersion compensation in modelocked lasers [8], time-wavelength spectroscopy [9,10], time-stretch analog-to-digital conversion [11,12], temporal imaging of optical pulses [13–16], and high-speed optical imaging [17,18]. Unfortunately, the devices used to generate large chromatic dispersion exhibit significant tradeoffs between GVD and other performance metrics. Pairs of diffraction gratings commonly used in CPA laser systems can offer large dispersion but at the expense of footprint because the GVD scales approximately linearly with the grating separation. Dispersion compensating fiber can provide a large amount of GVD in a small footprint, but has limited power-handling capability due to its large effective optical nonlinearity. More importantly, the use of dispersion compensating fiber is limited to the near-infrared telecommunication wavelength (~1550 nm) band. At other wavelengths, commercial optical fibers have large losses and limited dispersion. Chirped fiber Bragg gratings can produce large GVD, but suffer from similar power handling limitations due to their singlemode operation, and typically operate over a limited bandwidth within the telecommunication band.

Here, we demonstrate a new type of dispersive device that combines the spatial dispersion of diffraction gratings with the modal dispersion of a multimode waveguide to overcome the footprint, power, wavelength, and bandwidth limitations of conventional dispersive elements. This device, which may aptly be called the chromo-modal dispersion device (CMD), maps different wavelength components of an optical waveform to distinct modes of a multimode waveguide. The CMD then exploits the large modal dispersion inherent in a multimode waveguide to create chromatic dispersion (GVD).

An illustration of the generalized CMD is shown in Fig. 1. A broad-bandwidth optical pulse is incident on a pair of parallel diffraction gratings, which spatially disperses and collimates the pulse spectrum. The dispersed pulse propagates through a lens, which focuses the various spectral components at a range of angles relative to the optic axis. By placing the tip of a multimode fiber at the focus of the lens, each spectral component of the pulse excites

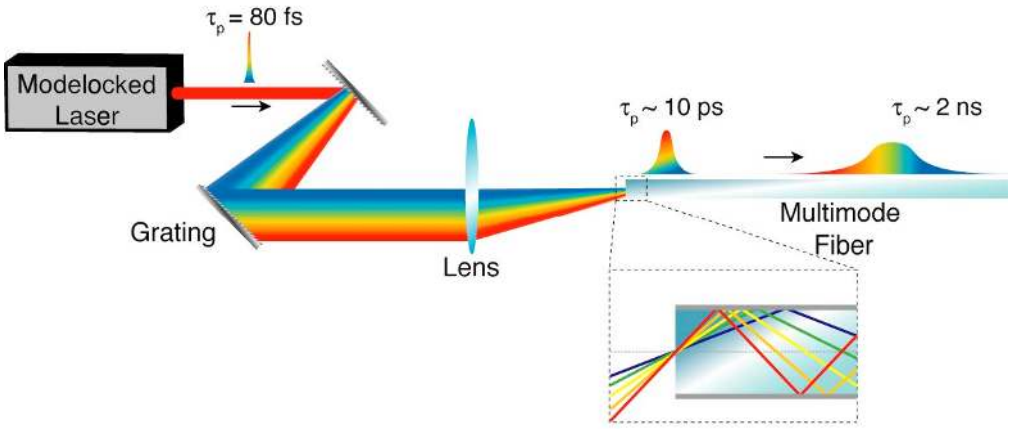

Fig. 1. Schematic diagram of the chromo-modal dispersion (CMD) device. Light is incident upon two parallel plane gratings, which disperse and collimate the optical spectrum. Angular dispersion is then applied to the spectrum using a lens. The input facet of a multimode fiber is placed at the lens focus such that the various spectral components are coupled into different fiber modes. The figure inset illustrates how different spectral components are coupled into and propagate in the multimode fiber. The dashed line represents the optic axis of the fiber. Although the configuration shown provides anomalous dispersion, the CMD can be tuned throughout both the anomalous and normal dispersive regimes by adjusting the alignment of the lens and fiber relative to the spatially dispersed spectrum.

#155170 - $15.00 USD Received 26 Sep 2011; revised 21 Oct 2011; accepted 23 Oct 2011; published 8 Nov 2011

a different mode of the optical fiber. Modal dispersion in the fiber imparts either normal or anomalous GVD to the pulse, depending on the transverse alignment of the lens relative to the spatially dispersed spectrum.

The CMD's use of large-core multimode fiber drastically reduces the undesirable effective optical nonlinearity, making it capable of handling much larger peak optical power than singlemode fiber-based dispersive devices. Additionally, the total footprint and size of the gratings used by the CMD are orders of magnitude smaller than grating-based Treacy-geometry dispersive elements with similar dispersion. Finally, since the CMD's operation is based on the wavelength-invariant principles of ray optics, it can operate at any wavelength for which multimode and transparent waveguides can be constructed.

2. Results

As a demonstration of the CMD's functionality, we characterize its dispersion in the 800-nm wavelength band. This is an especially important wavelength band for many biological applications because of its large penetration depth in tissues, which decreases at shorter wavelengths due to Rayleigh scattering and at longer wavelengths due to water absorption. Furthermore, this wavelength band is accessible by powerful and tunable modelocked Ti:sapphire lasers, which should enable the CMD to find use in a variety of biomedical, spectroscopic, and material processing applications.

In this work, we utilize two different implementations of the CMD (see Methods), making use of the fact that the device parameters (alignment, grating groove density, grating spacing, lens numerical aperture, fiber length, fiber numerical aperture) can be adjusted to modify its dispersive properties. To measure the dispersion of the CMD, we utilize the modulation phase shift method [19]. Using a radio-frequency lock-in amplifier as a phase-sensitive detector, we measure the relative phase shift between a 30-MHz amplitude-modulated continuous wave Ti:sapphire laser signal after it has traveled through CMD, and the reference 30-MHz signal used to drive the electro-optic modulator. By tuning the laser wavelength, we measure the wavelength-dependent phase delay of the CMD. To calculate the relative time delay (in ps) as a function of wavelength, we use the equation

$$\Delta\tau_\lambda = -\frac{\phi_\lambda - \phi_{\lambda_0}}{360 f_m} 10^{12}$$

where $\Delta\tau_\lambda$ is the time delay of a given wavelength, ϕ_λ is the relative phase of the signal at a given wavelength measured by the lock-in amplifier, and f_m is the amplitude modulation frequency. λ_0 is an arbitrary wavelength, which is chosen to have zero relative phase delay. A 3rd-order polynomial least-squares fit of the time delay data is used to calculate the dispersion parameter D_λ using

$$D_\lambda = \frac{d\Delta\tau_\lambda}{d\lambda}.$$

The results of these measurements and calculations are shown in Fig. 2. Additionally, to demonstrate the tunability of the CMD, we record several relative delay curves at different lateral positions of the focusing lens relative to the diffraction gratings. By maintaining alignment of the fiber tip at the lens focus, it is possible to tune the entire delay curve including zero-dispersion wavelength of the CMD. For the three alignment positions measured, the zero-dispersion wavelengths are 788.7 nm, 799.3 nm and 808.5 nm (curves 1, 2 and 3, respectively).

The CMD achieves large, tunable GVD by mapping the optical spectrum into modes of a multimode fiber. To confirm that different wavelengths occupy distinct transverse modes in the fiber, we measure the far-field mode profiles of the CMD output fiber as a function of excitation wavelength. Using the alignment position that yields the dispersion curve #1 in

#155170 - $15.00 USD Received 26 Sep 2011; revised 21 Oct 2011; accepted 23 Oct 2011; published 8 Nov 2011

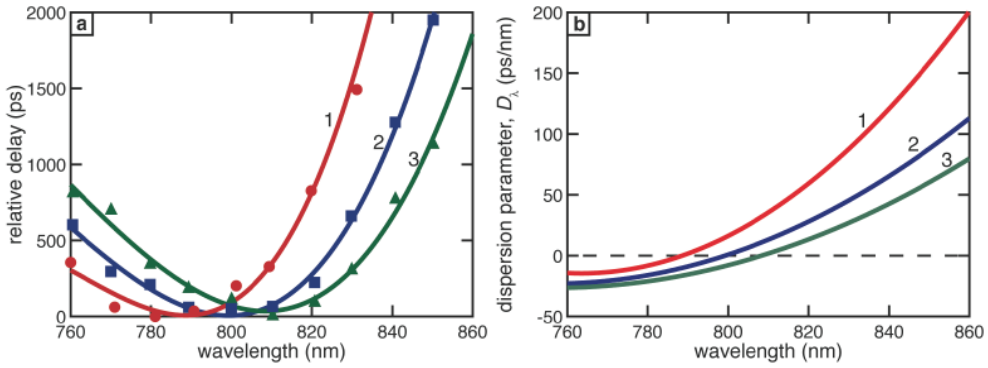

Fig. 2. (a) Relative delay and (b) dispersion parameter for three different alignments of the CMD. Translating the lens and fiber facet in the horizontal direction relative to the incident spatially dispersed spectrum shifts the CMD's zero dispersion wavelength.

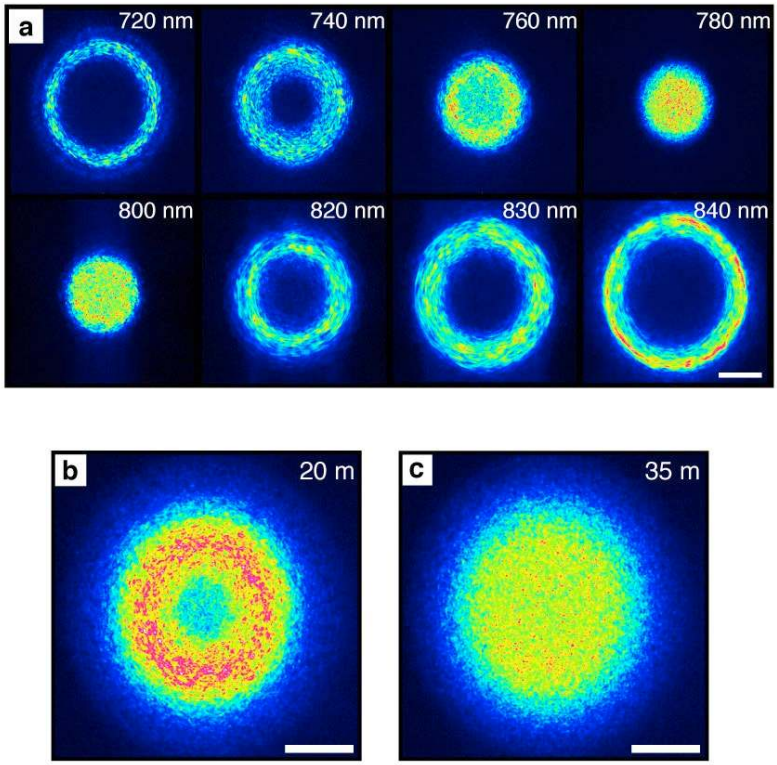

Fig. 3. Mode profiles at the output of the CMD fiber for alignment position #1, measured 5 mm from the output fiber facet. (a) Mode profiles recorded using various excitation wavelengths. (b) Mode profile using 745-nm excitation after propagating through 20 m of 200-μm core diameter fiber. (c) Mode profile using 745-nm excitation after propagating through 35 m of the same fiber. Blurring in the output mode profile indicates the coupling length has been reached. The scale bar in all cases is 1 mm.

Fig. 2(b), we record the mode profiles at various wavelengths using a CCD array placed 5 mm from the output tip of the fiber. The mode profiles for various excitation wavelengths are shown in Fig. 3(a).

Ideally, the CMD operates on the principle that individual wavelengths excite distinct modes of the multimode waveguide, each of which possesses a different propagation constant.

#155170 - $15.00 USD Received 26 Sep 2011; revised 21 Oct 2011; accepted 23 Oct 2011; published 8 Nov 2011

To achieve maximum dispersion for a given waveguide length, it is important to avoid mode coupling which can result from random inhomogeneity or bends in the fiber [20,21]. As a result, the coupling length sets an upper bound on the length of the fiber and hence, the maximum dispersion. Figures 3(b) and 3(c) show the far-field mode profile of the CMD measured at the end of a 20-m and 35-m lengths of fiber, respectively (using 745-nm excitation). As shown in Fig. 3(c), in the 35-m fiber the mode profile changes dramatically, indicating that the coupling length has been exceeded.

To measure the dispersive effect of the CMD on an optical pulse, we propagate pulses from a modelocked Ti:sapphire laser through the device, and monitor the fiber output using a fast photodiode (see Methods). The Ti:sapphire laser emits pulses (τ_{FWHM} = 80 fs, λ_{center} = 812 nm, $\Delta\lambda$ = 15.8 nm, repetition rate = 90.8 MHz) which are coupled into the CMD. By varying the alignment, the dispersion is tuned such that the entire pulse bandwidth lies in the anomalous ($D_\lambda > 0$) dispersion regime (Fig. 4(a)). As shown in Fig. 4(b), the time-domain output's full-width at half-maximum and full-width are 634 ps and 1.9 ns, respectively.

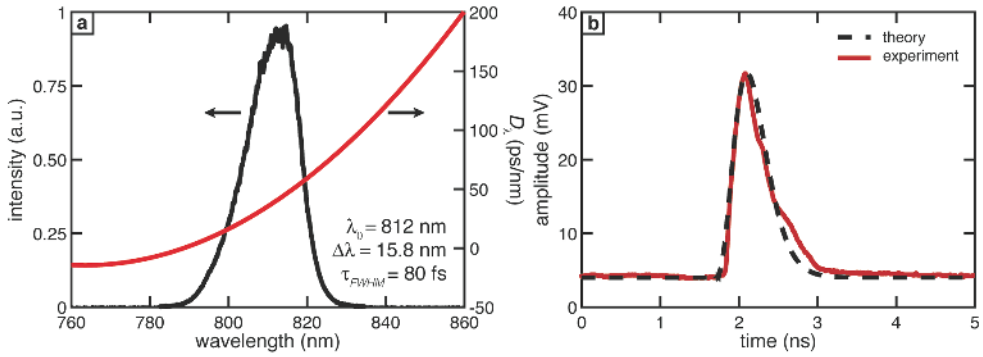

Fig. 4. Time-domain profile and spectrum of an 80-fs optical pulse after propagation through the CMD. (a) Spectrum of the input optical pulse and the CMD dispersion parameter. (b) Measured time-domain output (red) and calculated time-domain profile for the measured input spectrum and dispersion curve.

For comparison to the experimentally measured time-domain data, we simulated the dispersive propagation of a Gaussian optical pulse through the CMD. The simulated Gaussian pulse and CMD dispersion were chosen to have the same values as those used in the time-domain measurements. We performed the simulation by adding the appropriate spectral phase to the pulse in the frequency domain, and performing an inverse Fourier transform to return the data to the time domain. The calculated time-domain profile is denoted by the dashed curve in Fig. 4(b), which is in excellent agreement with the experimental measurement. Differences between the experimental and calculated plots of the time-domain data shown in Fig. 4(b) are attributed to both the use of an ideal Gaussian pulse spectrum and the use of a fit to the relative delay data, instead of the experimental values shown in Figs. 4(a) and 2(a).

Loss measurements were performed by monitoring the average power before and after the grating pair, and at the output of the CMD fiber. Using a modelocked Ti:sapphire laser with the CMD in alignment position #1, the diffraction gratings' loss was 6.0 dB. The loss due propagation through the lens and fiber was 1.52 dB. The large grating loss is due to the use of gratings not optimized for operation at 800 nm, and can be reduced to approximately 0.4 dB by using high-efficiency dielectric gratings [22]. There was no observable spectral dependence of the loss due to propagation through the fiber, as the mode-dependent attenuation is negligible for 20 m of this fiber.

To demonstrate another application of the CMD in a wavelength range outside the telecommunication band, we performed real-time, single-shot [9,23,24] time-wavelength atomic absorption spectroscopy of the D_2 ($5^2S_{1/2} \rightarrow 5^2P_{3/2}$) transition in rubidium vapor. In

#155170 - $15.00 USD Received 26 Sep 2011; revised 21 Oct 2011; accepted 23 Oct 2011; published 8 Nov 2011

this experiment, near-transform-limited pulses from a modelocked Ti:sapphire laser (λ_{center} = 780 nm, $\Delta\lambda$ = 35 nm, repetition rate = 90.8 MHz) were transmitted through a 225-mm path length rubidium vapor cell before entering a CMD optimized for anomalous dispersion over a 4-nm bandwidth (see Methods). The optical spectrum transmitted through the CMD and the associated time-domain signals are shown in Figs. 5(a) and (b), respectively. Spectra are recorded by an oscilloscope in this fashion every 11.01 ns, which is orders of magnitude faster than is possible using conventional array-detector- or scanning-based spectrometer. In addition, the effective spectrometer shutter speed, or integration time, of this measurement is equal to the optical transit time through the rubidium cell, which is approximately 750 ps. In this spectroscopy experiment, the Doppler-broadened D_2 transition in rubidium generates an absorption dip in the transmission spectrum, which is observed in the time-domain profile. While it is clear from the experimental data that the CMD produces a time-wavelength mapping, it is also important to note that in this case, the amount of dispersion is sufficient to satisfy the uncertainty principle requirement for generating a dispersive Fourier transform of the wavelength-domain signal [25,26].

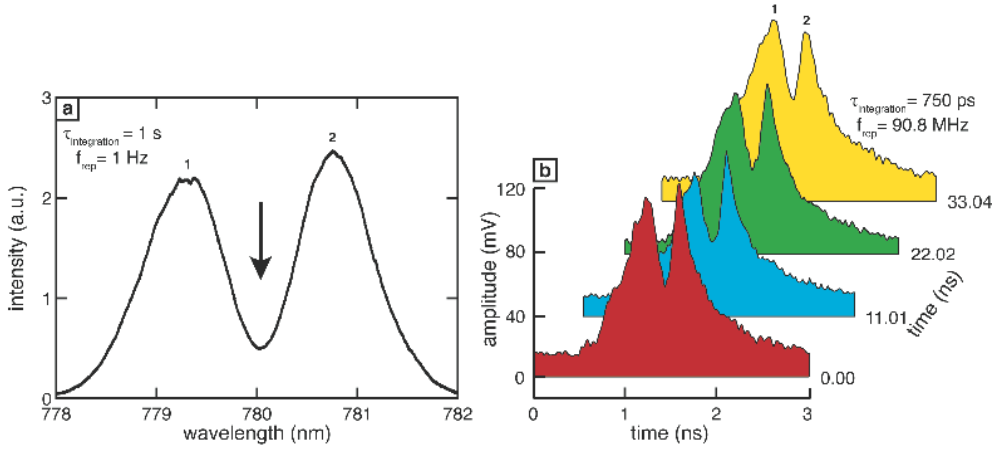

Fig. 5. Single-shot atomic absorption spectroscopy of rubidium vapor. (a) Optical spectrum after passing though the rubidium cell and the CMD, as measured by a conventional spectrometer. The arrow represents the position of the Doppler-broadened D_2-absorption line. (b) Sequence of four consecutive single-shot time-domain traces captured by a photodiode and oscilloscope at a repetition rate of 90.8 MHz. High-frequency amplitude noise in the time-domain signals is a result of ringing in the measurement, and is not fundamental to the time-wavelength spectroscopy technique. The horizontal time axis can be converted to wavelength with knowledge of the CMD dispersion curve. Peaks "1" and "2" are denoted in both (a) and (b) to illustrate correspondence in the time-wavelength mapping.

3. Discussion

The multimode fiber used in this work supports a number of modes, *M*, which can be approximated as [27]

$$M \approx \frac{V^2}{2},$$

where the V-number is defined as

$$V = \frac{2\pi}{\lambda} a \cdot \mathrm{NA}$$

where *a* is the fiber core radius and NA is the fiber numerical aperture. For a wavelength of 800 nm, fiber core diameter of 200 μm, and NA of 0.37, approximately 42200 allowed fiber eigenmodes exist. As a result of this large number of modes and the finite bandwidth of the

#155170 - $15.00 USD Received 26 Sep 2011; revised 21 Oct 2011; accepted 23 Oct 2011; published 8 Nov 2011

optical detection system (see Methods), optical pulses dispersed using a CMD possessing this number of modes will exhibit a smooth time-domain profile, such as shown in Fig. 4(b). The total dispersion generated by this CMD is not sufficient to enable resolution of the individual modes in the time domain.

Fundamentally, the mode coupling length and the numerical aperture (NA) of the multimode fiber determine the maximum dispersion of the CMD. For fiber lengths shorter than the coupling length, modal dispersion dictates that the maximum output pulsewidth of the CMD can be approximated by [27]

$$\Delta\tau_p = L\frac{N_2}{c}\left(\frac{n_1 - n_2}{n_2}\right)$$

where $\Delta\tau_p$ is the output pulsewidth, L is the fiber length, n_1 and n_2 are the material refractive indices of the fiber core and cladding, respectively, and N_2 is the group index of the cladding. For an input pulse with a center wavelength of 800 nm propagating in a 20-m long pure silica core fiber with a 0.37 NA, the maximum output pulsewidth is approximately 3 ns, assuming all modes of the fiber are excited. A noteworthy feature of CMD is that the output pulsewidth is independent of the input optical bandwidth, provided that it is sufficiently spatially dispersed to intercept the entire NA of the fiber after being focused by the lens. Thus, the CMD is capable of stretching small-bandwidth pulses by a large amount in a small footprint. As an example, we consider a device consisting of two 30-mm wide, 2200 line/mm gratings spaced by 10.8 cm (aligned for an angle of incidence of 50 degrees from the grating normal), a 25.4-mm diameter 0.37-NA lens, and 20-m of 0.37-NA step-index multimode fiber. For an optical pulse of 1-nm bandwidth centered at 800 nm, this CMD can provide approximately ± 3000 ps of group delay, stretching an 800-nm center wavelength, 1-ps pulse to a duration of 3 ns. To achieve the same dispersion, two gratings with the same groove density placed in a double-pass Treacy geometry [28] would have to be spaced by 1400 cm, and one grating would have to be greater than 25 cm in width. The ability to impart large normal or anomalous dispersion over a small optical bandwidth makes the CMD invaluable for applications in picosecond CPA laser systems, which traditionally employ large-footprint, grating-based stretchers and compressors [28–30]. Finally, in contrast to single mode dispersive fibers, the CMD is much better suited for accommodating high optical power without introducing distortions caused by optical nonlinear interactions. This is a direct result of the large cross section of the multimode fiber, which reduces its effective nonlinearity. This feature can be further improved by replacing the fiber with a hollow multimode waveguide such as those previously reported [31].

As shown in Fig. 3(a), the spectrum of the input pulse defines the output mode profile, which can differ significantly from the input mode. To circumvent this mode-conversion in applications such as CPA, in which the pulse stretcher and compressor spatial modes are critical, one may use a length of fiber in the CMD slightly longer than the coupling length. Coupling the modes using an extended length of fiber generates an output that consists of the sum of all fiber mode profiles (Fig. 3(c)), as opposed to only modes excited initially (Fig. 3(b)). Higher-order modes can subsequently be suppressed, *e.g.* using fiber coiling [32] or other techniques [33,34] which reduce the output beam's M^2 value. The resulting optical loss due to filtering can be compensated using signal post-amplification techniques [17,18].

For applications in which the output spatial mode is less important than the time-domain profile, such as in the time-wavelength spectroscopy experiment reported here, it is imperative that the CMD fiber length remains shorter than the fiber coupling length. As shown in Fig. 5, the CMD generates a wavelength-to-time mapping of the optical spectrum used to probe the D_2 transition in rubidium vapor in real-time. Nonlinearity in this mapping can be attributed to the shape of the CMD's dispersion curve, which is fundamentally the same as that shown in Fig. 2(b), albeit over a bandwidth of ~4 nm. This nonlinearity in the

#155170 - $15.00 USD Received 26 Sep 2011; revised 21 Oct 2011; accepted 23 Oct 2011; published 8 Nov 2011

CMD's dispersion slope is static and deterministic, and hence, it can be compensated using digital post-processing [35–37]. Thus, knowledge of the CMD dispersion combined with the appropriate laser source and detector will enable high spectral resolution, real-time spectroscopy at any wavelength for which the fiber is transparent or a hollow waveguide can be constructed.

4. Conclusion

In summary, we have demonstrated and characterized a compact device that produces large and tunable group velocity dispersion. This has been achieved by transforming the large modal dispersion of a multimode fiber into chromatic dispersion. The amount of dispersion as well as the zero dispersion wavelength is tunable and produces normal or anomalous dispersion, with maximum dispersion limited only by the coupling length and NA of the multimode fiber used. As a proof of concept demonstration, we stretch a sub-picosecond optical pulse to nearly 2 ns in 20 m of multimode optical fiber. By adjusting the grating groove density and separation, The CMD can be configured to accommodate larger or smaller bandwidth pulses, while maintaining the same output pulse width. To demonstrate one of its utilities, we demonstrated single-shot atomic absorption spectroscopy of rubidium vapor. The large dispersion and small footprint of the device make the CMD potentially useful for on-chip dispersion compensation using optical components such as integrated gratings and planar multimode waveguides. The CMD's physical compactness, combined with the magnitude and tunability of its dispersion suggest its use as a versatile tool for pulse stretching or compression in a variety of applications in which the capabilities of singlemode fiber or diffraction grating-based dispersive elements will not suffice.

5. Methods

The CMD used in all experiments except for absorption spectroscopy is constructed from a pair of 900-grooves/mm ruled diffraction gratings spaced 14 cm apart, a f = 35 mm, 25.4-mm diameter, antireflection-coated achromatic doublet lens, and a 20-m long, 200-μm diameter core, 0.37-NA step-index pure silica core, polymer cladding multimode optical fiber. The lens and fiber are mounted on the same linear translation stage, such that as the transverse alignment of the lens is altered, the fiber tip remains at the focus of the lens. Modulation phase shift measurements were performed using a custom-built continuous wave Ti:sapphire laser. The laser linewidth full width at half maximum for each measurement point was less than 0.20 nm. The RF lock-in amplifier time constant was set to 1 second for all measurements. Time-domain measurements were performed by connecting an unamplified InGaAs photodiode with a 25-ps impulse response time to the output of the CMD. Electrical signals from the photodiode are recorded using a 50-gigasample/s, 16-GHz analog bandwidth oscilloscope. Real-time atomic absorption spectroscopy was performed on a heated 75-mm length rubidium vapor cell (natural isotope mixture) in a triple-pass geometry. A narrow bandpass filter ($\Delta\lambda$ = 3 nm) centered at 780-nm was placed after the rubidium cell to limit the optical bandwidth entering the CMD. The CMD configuration used in this experiment consisted of two 30-mm length, 2000 grooves/mm ruled diffraction gratings spaced by 28 cm. The lens and fiber were the same as used in all other experiments.

Acknowledgments

E. D. D. and B. J. conceived the design of the CMD. J. C. and T. S. performed initial simulations of the device. E. D. D., N. K. H., Z. T., and C. W. performed the experiments and data analysis. E. D. D. wrote the first draft of the manuscript.

#155170 - $15.00 USD Received 26 Sep 2011; revised 21 Oct 2011; accepted 23 Oct 2011; published 8 Nov 2011